Supporting Information for "Sensitivity of deep ocean mixing to local internal wave breaking and mixing efficiency"

Laura Cimoli[1], Colm-cille P. Caulfield[2], Helen L. Johnson[3], David P.

Marshall[1], Ali Mashayek[4], Alberto C. Naveira Garabato[5], Clément Vic[6]

[1]Department of Physics, University of Oxford

[2]BP Institute & Department of Applied Mathematics & Theoretical Physics, University of Cambridge

[3]Department of Earth Science, University of Oxford

[4]Civil and Environmental Engineering, Grantham Institute of Climate and Environment, Imperial College

[5]National Oceanography Centre, University of Southampton

[6]Univ. Brest, CNRS, IRD, Ifremer, Laboratoire dOcéanographie Physique et Spatiale (LOPS), IUEM, Plouzané, France

Contents of this file

1. Figures S1 to S8

Introduction

This supporting information contains the following figures and information:

• Figure S1: global map of buoyancy Reynolds number (Re_b) at the depth of 3500 m calculated by using a variable breaking efficiency $q(x, y)$. From the parameterization of the flux coefficient used in this study (see Figure 1f), the maximum flux coefficient

October 26, 2019, 9:50pm

$\Gamma(Re_b)$ is found when $Re_b = 100$ (red contour in Figure S1). The patterns of Re_b provide insights into understanding the pattern of the flux coefficient: the flux coefficient peaks at $Re_b = 100$, while regions of lower and higher Re_b feature weaker flux coefficients, implying that waters are mixed less efficiently. The mixing efficiency is reduced mainly because either the turbulence is not strong enough ($Re_b < 100$, left side of the curve in Figure 1f), or because stratification is too weak ($Re_b > 100$, right side of the curve).

• Figure S2: Figures S2a and S2b show respectively the power from locally breaking internal tides, P_{loc}, and the dissipation rate, ϵ, at the depth of 3500 m calculated by using a variable local breaking efficiency $q(x, y)$ and a variable flux coefficient $\Gamma(Re_b)$. Both P_{loc} and ϵ are enhanced close to complex topographic structures, i.e. where the energy conversion into internal tides is stronger.

• Figure S3: differences in diapycnal velocities between the cases (q) and (q_c), the latter being the case where q is geographically constant, but adjusted such that the energy rate from locally breaking waves in the two cases is the same (and so $q_c = 0.4739$). Figure S3a shows the differences in diapycnal upwelling, and Figure S3b shows the differences in diapycnal downwelling.

• Figure S4: both $q(x, y)$ and $\Gamma(Re_b)$ have uncertainties that can affect our results. Therefore, we discuss here the choices of parameters used and their uncertainty, and we show in Figures S4a and S4b the sensitivity of the net water mass transformation rate to changes in $q(x, y)$ and $\Gamma(Re_b)$, respectively.

The map of $q(x, y)$ depends on the cutoff mode number used to partition the near-field to the far-field energy available to mixing. The cutoff mode number depends both on the

attenuation length scale of mode-1 internal tides and the resolution of the grid used to compute the energy conversion and design the parameterization for near-field dissipation. The sensitivity of $q(x, y)$ to the cutoff mode number and the grid resolution is discussed in the Supplementary Note 4 in Vic et al. (2019). They show that $q(x, y)$ is poorly sensitive to values of the critical mode number in [3, 4, 5], due to the very strong conversion occurring in high modes (notably, modes > 10), compared to the individual contributions of modes 3, 4 or 5. Based on their Supplementary Figure 5, point-wise $q(x, y)$ would change by roughly 15% for critical mode numbers of 3 or 5 instead of 4. In Figure S4a we show that changing $q(x, y)$ by 15% changes the net water mass transformation by < 1 Sv.

The sensitivity of the water mass transformation rate to the choice of parameters used to infer the flux coefficient $\Gamma(Re_b)$ has been shown in Mashayek et al. (2017), whose parameterization for Γ is used here with minor modification. The results presented in this study have been produced using $\Gamma^* = 0.35$ and $Re_b^* = 100$. In Figure S4b we show the sensitivity of transformation rates to Γ^* and Re_b^* (both with a variable $q(x, y)$). The peak overturning rate (on the neutral density surface $\gamma^n = 28.1$) varies between 8-16 Sv depending on the choice of Γ^* and Re_b^*. Further progress in the field of density stratified turbulence is required to refine Γ^* and Re_b^*. For now, the choices of $\Gamma^* = 0.35$ and $Re_b^* = 100$ give the best fit to the available observational, experimental and numerical data as summarized in Mashayek et al. (2017); Monismith, Koseff, and White (2018).

• Figure S5: the different panels show the global average dissipation rate of turbulent kinetic energy, ϵ, flux coefficient, Γ, and buoyancy flux, $\mathcal{M} \approx \Gamma\epsilon$, as a function of height above the bottom for the different scenarios investigated here. The dissipation rate

decreases (Figure S5a) exponentially from the bottom, following the exponential decay scale used to calculate the power from locally breaking internal tides (equation 2). On the other hand, the flux coefficient is vertically non-monotonic (Figure S5b). It increases with depth as the turbulence increases, but decreases in the proximity of the bottom, where the stratification vanishes. The vanishing flux coefficient allows the buoyancy flux to be zero at the boundary (Figure S5c), satisfying the no-flux across the boundary condition.

• In this study, we have used a constant e-folding scale, ζ, for the vertical decay function $\mathcal{F}(z)$ (see equation 2), which describes the vertical distribution of the internal wave energy available for mixing. The value chosen, $\zeta = 500$ m, is motivated by observations of turbulence in the deep ocean, which is observed to decrease exponentially in the water column (St. Laurent et al., 2002). However, such decay is not expected to be spatially uniform, but to vary depending on the local topography, turbulence and stratification. Observation-constrained estimates of a variable $\zeta(x, y)$ are not available yet, and so the sensitivity of diapycnal mixing to a variable vertical energy distribution is not within the scope of this paper. However, to assess the potential effect of a variable $\zeta(x, y)$ on diapycnal mixing patterns and the global water mass transformation rate, we analyze here a separate case in which we use the spatially variable decay scale produced through realistic simulations from Melet, Hallberg, Legg, and Polzin (2013), shown in Figure S5. Their model output suggests a sharp decay of energy (100 - 500 m) in regions of enhanced turbulence and a smooth decay (up to 1500 m or more) in regions of low turbulence. The differences in diapycnal upwelling and downwelling between a constant and a variable decay scale is presented below in Figure S6 by comparing two cases: the case ($q\Gamma$), i.e.

where both the local breaking efficiency and the flux coefficient are represented as spatially variable, is compared with the case $(q\Gamma\zeta)$, i.e. in which also the decay scale is allowed to vary (while it was assumed constant, $\zeta = 500$ m, in the former case). Figure S7 shows the differences in diapycnal upwelling (panel (a)) and downwelling (panel (b)) between the two cases described above at the depth of 4000 m. The patterns of the differences in the diapycnal velocities show similarities with the map of the variable decay scale (Figure S6). Diapycnal upwelling/downwelling are enhanced in regions of sharp energy decay, i.e. where $\zeta(x, y) < 500$ m, and reduced in regions where $\zeta(x, y) > 500$ m. These differences have comparable orders of magnitude to the anomalies observed while changing q and Γ, and so cannot be neglected. The results suggest that a variable e-folding scale can significantly contribute to altering the patterns of diapycnal upwelling/downwelling, while the net rate of water mass transformation remains almost unchanged due to large cancellations between alterations to upwelling and downwelling regions (shown in Figure S8).

While the variable $\zeta(x, y)$ from Melet et al. (2013) is useful to explore the importance of how the vertical energy is distributed, observation-based estimates of $\zeta(x, y)$ are needed to quantify its impact on diapycnal mixing more accurately.

References

Mashayek, A., Salehipour, H., Bouffard, D., Caulfield, C., Ferrari, R., Nikurashin, M., . . . Smyth, W. (2017). Efficiency of turbulent mixing in the abyssal ocean circulation. *Geophysicasl Research Letters*, *44*, 6296-6306.

Melet, A., Hallberg, R., Legg, S., & Polzin, K. (2013). Sensitivity of the ocean state to

the vertical distribution of internal-tide-driven mixing. *Journal of Physical Oceanography*, *43*(3), 602–615.

Monismith, S. G., Koseff, J. R., & White, B. L. (2018). Mixing efficiency in the presence of stratification: when is it constant? *Geophysical Research Letters*, *45*(11), 5627–5634.

St. Laurent, L., Simmons, H., & Jayne, S. (2002). Estimating tidally driven mixing in the deep ocean. *Geophys. Res. Lett.*, *29*.

Vic, C., Garabato, A. C. N., Green, J. M., Waterhouse, A. F., Zhao, Z., Melet, A., ... Stephenson, G. R. (2019). Deep-ocean mixing driven by small-scale internal tides. *Nature communications*, *10*.
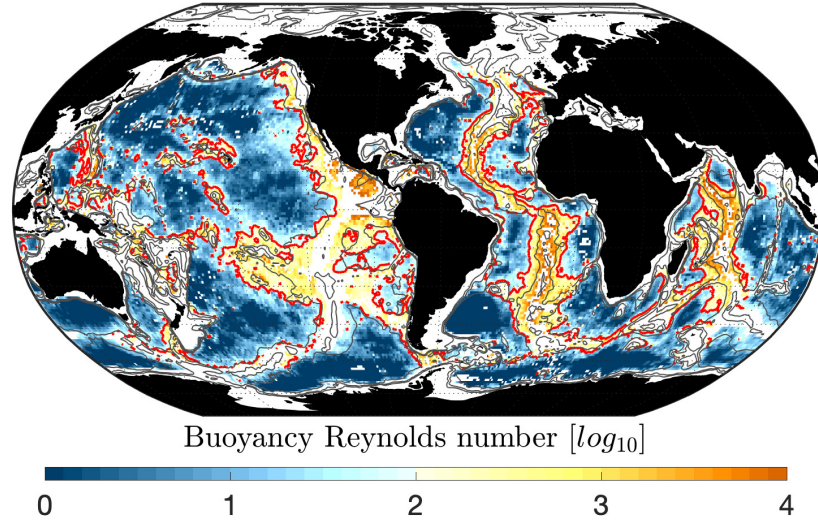
Figure S1. Global map of the buoyancy Reynolds number at 3500 m calculated by using a variable $q(x,y)$. The red contour identifies the points where $Re_b = 100$. The gray contours are the 2000, 3000 and 4000 m bathymetry contours.

$$\epsilon = \frac{P_{loc}}{\Gamma+1}$$
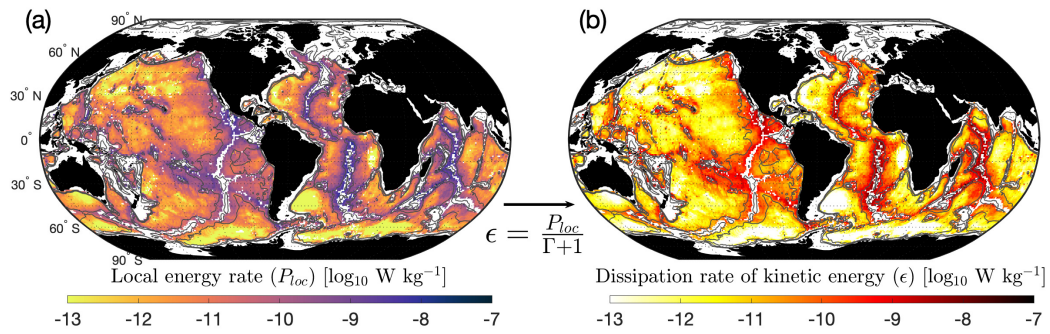
Figure S2. (a) Global map of rate of energy from locally breaking waves, P_{loc}, at 3500 m. (b) Global map of turbulent dissipation rate, ϵ, at 3500 m inferred from the global map of P_{loc} by using the relationship showed. Both panels have been produced using the spatially variable $q(x,y)$ and a spatially variable flux coefficient $\Gamma(Re_b)$.
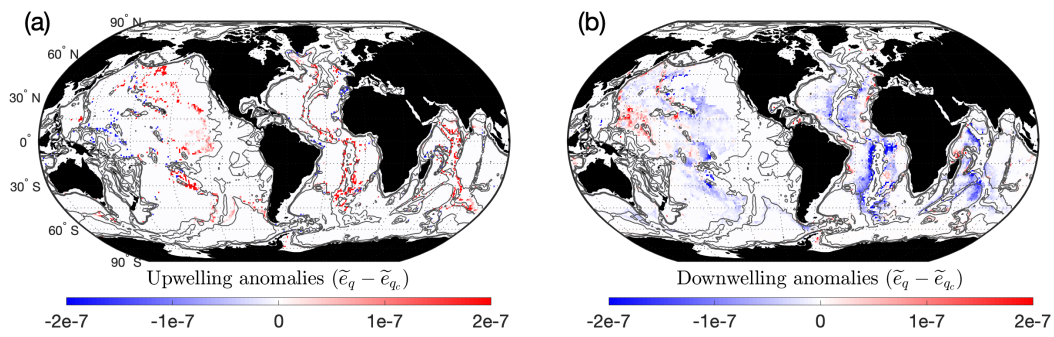
Figure S3. Differences in (a) diapycnal upwelling and (b) diapycnal downwelling between case (q) and (q_c). Units are m/s.
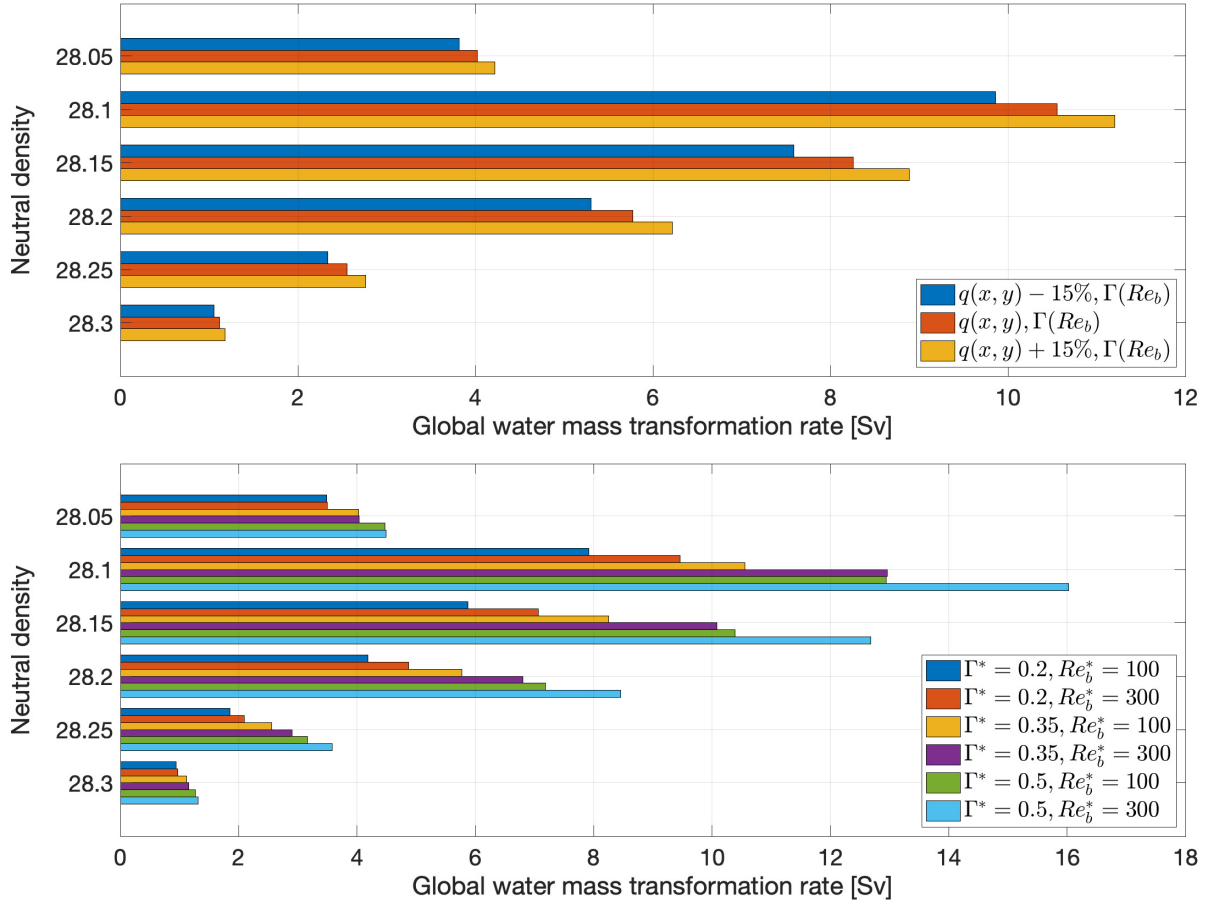
Figure S4. (a) Sensitivity of the net water mass transformation to changes in $q(x,y)$ by 15% (all the cases have been run with a variable flux coefficient). (b) Sensitivity of the net water mass transformation to different values of Γ^* and Re_b^* (all the cases have been run with a variable local breaking efficiency $q(x,y)$).
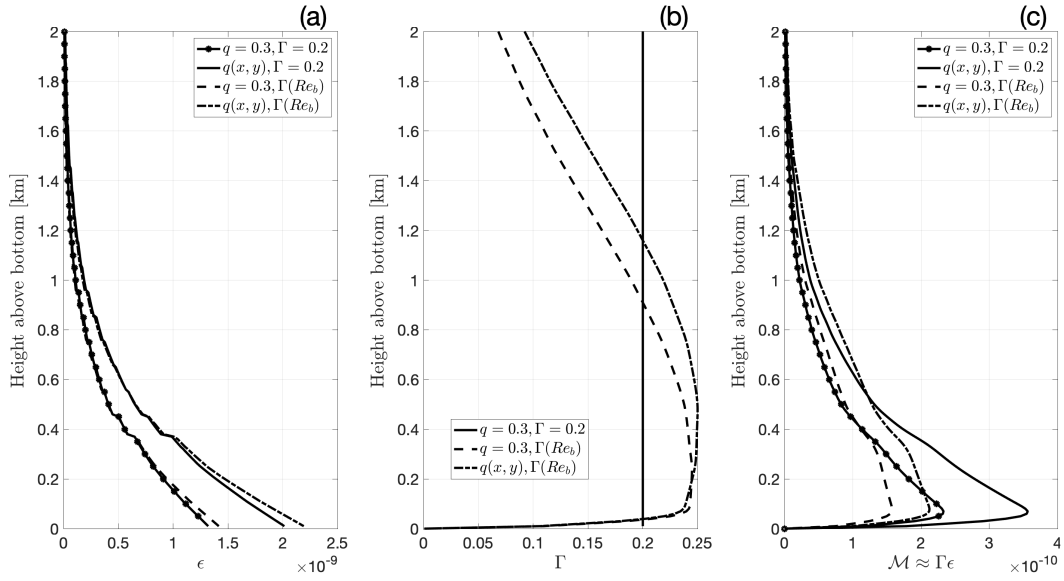
Figure S5. Global average (a) dissipation rate of turbulent kinetic energy, ϵ, (b) flux coefficient, Γ, and (c) buoyancy flux, $\mathcal{M} \approx \Gamma\epsilon$ for the different scenarios.
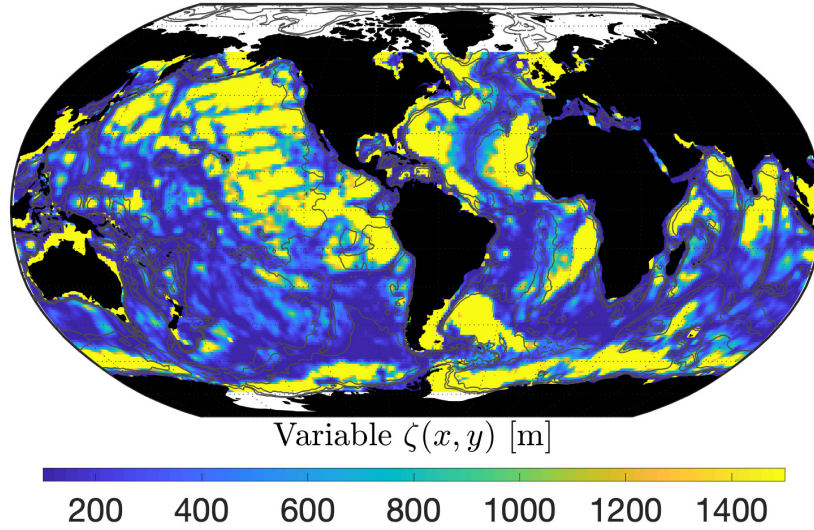

Figure S6. Global map of variable vertical decay scale $\zeta(x,y)$, reconstructed from Melet et al. (2013).
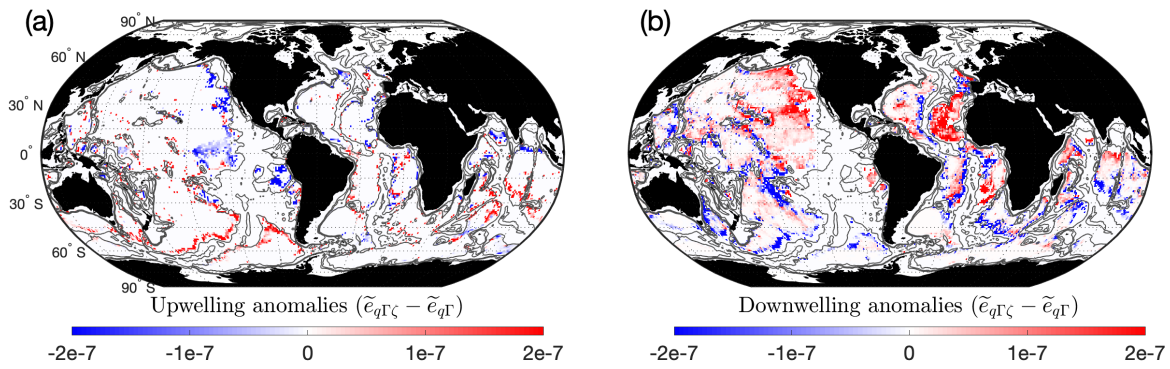
Figure S7. Differences in (a) diapycnal upwelling and (b) diapycnal downwelling between case $(q\Gamma\zeta)$ and $(q\Gamma)$. Units are m/s.
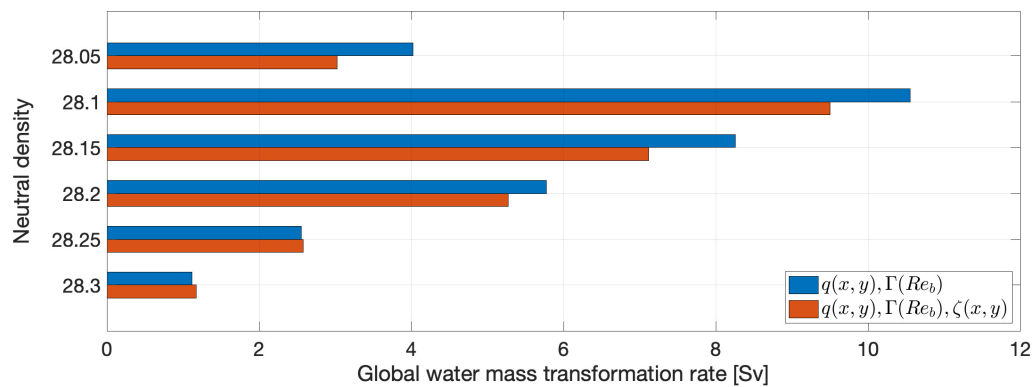

Figure S8. Total global water mass transformation for the cases $(q\Gamma)$, in blue, and $(q\Gamma\zeta)$, in red.